Scatter Correction by Modulation of Primary Radiation in Industrial X-ray CT: Beam-hardening Effects and their Correction

Karsten SCHÖRNER[*], Matthias GOLDAMMER[**], Jürgen STEPHAN[**]
[*]Corporate Technology, Siemens AG, 81739 München, Germany, and
Physik-Department E21, Technische Universität München, 85748 Garching, Germany
karsten.schoerner.ext@siemens.com, karsten.schoerner@tum.de
[**] Corporate Technology, Siemens AG, 81739 München, Germany
matthias.goldammer@siemens.com, juergen.stephan@siemens.com

Abstract. Scattered radiation presents a major cause of image degradation for industrial X-ray cone-beam CT scanners. It introduces several kinds of artifacts in reconstructed CT volumes, such as streaks, a general loss of contrast, and inhomogeneities in regions of homogeneous material, also known as cupping artifact. We present a novel experimental method for the correction of scatter artifacts which is adapted from medical application and based on primary modulation. Here, a primary modulator placed between the X-ray source and an object imprints a spatially varying pattern on primary X-rays through attenuation, e.g. a checkerboard-like pattern. This modulation pattern is only preserved in unaltered primary X-ray photons – scattered X-rays have a broad spatial distribution after the (Compton-) scattering process and, thereby, the original pattern gets lost. Thus, modulated primary signals and non-modulated scatter signals can be separated in frequency space by appropriate filtering algorithms. After demodulation of primary signals and their subtraction from total signals, we obtain a scatter estimate. For the proposed scatter correction method, we introduce a beam-hardening correction procedure and discuss its effects on the scatter estimation process. Scatter-corrected CT reconstructions show a significant improvement in image quality. Compared to other scatter correction techniques, e.g. approaches based on beam-stops, this method offers the advantage to integrate the scatter measurement into the actual CT scan which reduces scan time and effort.

Introduction

In recent years, industrial X-ray cone-beam computed tomography (CBCT) has become a major technique in non-destructive testing enabling precise visualization and inspection of a part's internal structures. While CBCT has become an increasingly important tool for industrial evaluation and inspection tasks it has found many applications in different industrial fields ranging from very small parts, e.g. chips or other tiny electronic components on printed circuit boards, to rather large samples, e.g. heavy parts from gas turbines including ceramic heat shielding structures [1] or turbine blades [2]. In CBCT scanners modern flat-panel detectors are used for complete 2D data acquisition at one time. While extending the volume coverage and thereby reducing scan time significantly, this also leads to an increased contribution of scattered radiation to the total detected signal.

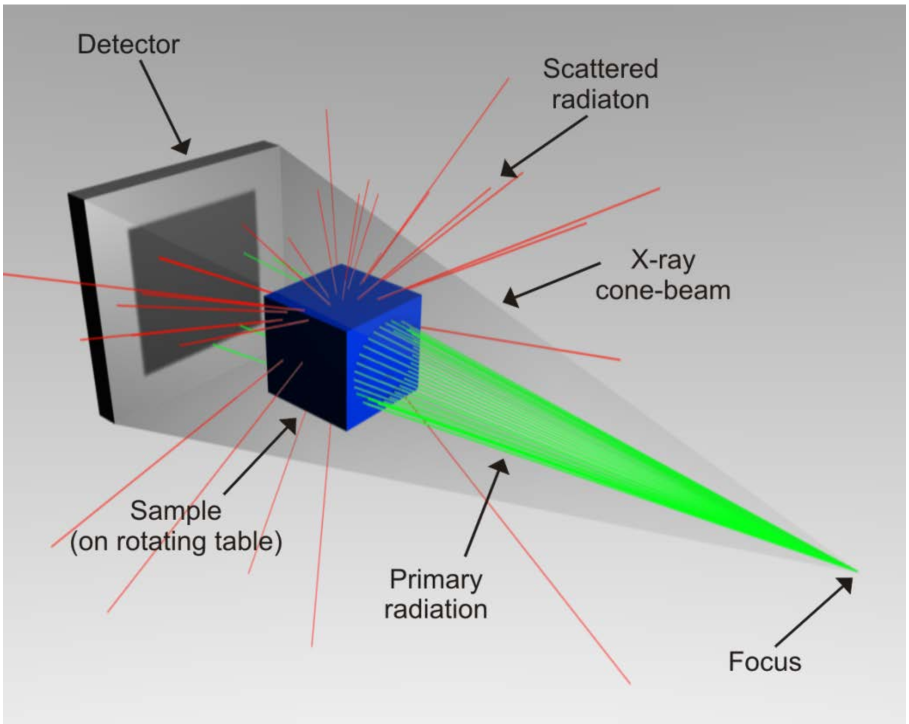

Figure 1. Schematic illustration of standard cone-beam CT setup with primary radiation partially scattered by the sample. Part of the scattered radiation reaches the detector where it gives rise to secondary signals, leading to scatter artifacts in reconstructed CT volumes, e.g. streaks, cupping artifact, and loss of contrast.

Scattered radiation presents a major source of image degradation in CBCT systems introducing typical scatter artifacts to reconstructed CT volumes such as cupping in homogeneous regions of material [3], loss of contrast, as well as streaks between regions of high contrast [4]. Additionally, image noise is increased if scattered radiation is not removed before impinging on the detector [5]. Also, dimensional measurements are negatively affected by scatter since it blurs sharp edges and renders flat surfaces bent in the surface detection step [6]. Accordingly, for large-scale samples which are tomographed with small magnification, i.e. which are located close to the detector, these artifacts become even more severe. Figure 1 schematically illustrates such a situation within a standard CBCT setup where primary radiation (green) is partially scattered (red) by the sample. A fraction of the scattered radiation reaches the detector plane giving rise to (secondary) scatter signals there.

In the field of medical CT, numerous approaches for scatter suppression as well as methods for scatter correction have been developed. Scatter suppression aims at reducing the number of scattered photons reaching the detector, e.g. by use of an anti-scatter grid [5] or increased air gaps [7]. While this can reduce the amount of detected scatter, it does not eliminate it completely. By contrast, scatter correction methods can be applied a posteriori to subtract the scatter contribution from the total detected signal. This requires precise knowledge of the scatter distribution in each projection. Several software-based scatter estimation methods exist which can be divided into calculations based on analytical scatter models, Monte-Carlo simulations, and hybrid methods.

Apart from software-based methods, we want to point out two different experimental approaches which aim at measuring the scatter signal at a number of sampling points. The first group includes beam-stop based techniques such as the beam-stop array (BSA) and a complementary method using apertures which we call beam-hole array (BHA) [1,8,9]. In both techniques, highly absorbing elements (tungsten or lead) are used to either totally block primary signals (BSA) or to eliminate scatter signals (BHA) for a number of small sampling points. In either case, a second scan without BSA/BHA is required in order to

obtain complete projection data for the entire field-of-view. While these techniques lead to significant improvement in image quality, both the BSA and BHA method necessitate additional scan time, measurement effort as well as additional dose.
Besides the mentioned experimental methods, recently, Bani-Hashemi *et al.* and Zhu *et al.* have proposed a new scatter correction method for medical applications based on the spatial modulation of primary radiation [10,11]. The concept of spatial primary modulation (SPM) allows for complete integration of scatter data acquisition into the normal CT scan whereby additional scan time and effort are made obsolete. This constitutes a great advantage of the proposed method.
In this work, we want to discuss how SPM can be implemented in an industrial CBCT scanner. Specifically, we consider beam-hardening effects which are caused by primary modulators inserted into the beam path and which result in incorrect scatter estimates. Eventually, we present preliminary CT results which illustrate a promising capability of this method to correct scatter artifacts by SPM while not extending scan time and effort.

1. Theory

1.1 Concept of Spatial Primary Modulation

Scatter correction by spatial primary modulation (SPM) is theoretically discussed in [10] and experimentally tested in [11]. Here, we want to give a brief explanation of its underlying concept. The fundamental aim of SPM is to obtain an estimate of the primary image, and subsequently, to subtract this estimate from the total projection in order to obtain a scatter estimate for each CT projection. This is achieved by insertion of a so-called primary modulator into the X-ray cone-beam between sample and X-ray tube, which imprints a regular spatial attenuation pattern onto the primary radiation before it passes the sample. Let us consider an attenuation pattern in the form of a checkerboard with transparent (bright) and semi-transparent (dark) squares. While this spatial pattern is preserved by primary X-rays, photons which are scattered by the sample (mostly due to Compton scattering processes) will have new directions of propagation and thereby will smear out the pattern which leads to a diffuse scatter signal S of low spatial frequency on the detector. Consequentially, this scatter contribution S is assumed to be unmodulated and low-frequency. It is superimposed by the low-frequency part of primary radiation P. As Fig. 2 illustrates, in Fourier space these overlapping contributions $P+S$ are located near the center (where spatial frequency is zero) thereby exhibiting low-frequency character. On the other hand, modulated primary radiation gives rise to modulated primary signals P on the detector. Since primary X-rays at the detector plane have not undergone any interaction with the sample and, thus, have not been deflected, they still will show the modulation imprint. In fact, these signals represent the result of multiplication of the spatial attenuation function of the object with the spatial modulation function. In frequency space, this corresponds to the convolution of the object attenuation function's frequencies with the modulation function’s frequencies. The latter features dominant frequencies, i.e. modulation frequency f_{mod} (given by the reciprocal of the spatial period of the modulation pattern) plus its multiples. Therefore, spectral copies of exclusively primary signals P are found around the modulation frequencies in 2D Fourier space as shown in Fig. 2 bottom right. Thus, separation in frequency space of modulated primary signals and unmodulated primary plus scatter signals through appropriate filtering algorithms facilitates estimation of the primary image and lies at the heart of the concept of SPM.

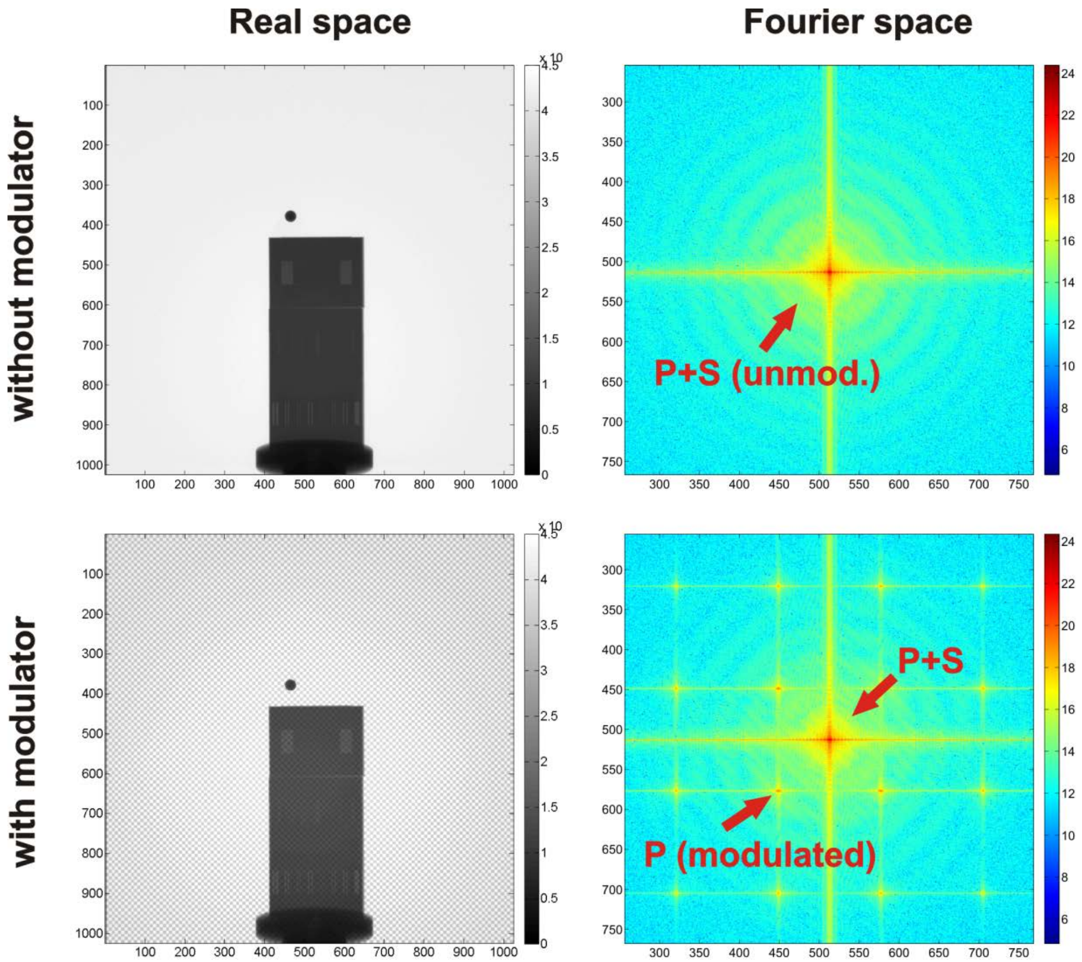

Figure 2. Conceptual illustration of spatial primary modulation. Top: In a normal CT projection, without primary modulator, total signals are given by the sum of primary and scatter signals, $P+S$. Fourier-transformation of this projection yields the 2D power spectrum on the right-hand side where primary and scatter signals particularly overlap in the low-frequency regions located near the center.
Bottom: Same CT projection with primary modulator inserted in front of object. The regularly spaced pattern of the primary modulator imprints an attenuation pattern onto the primary radiation which leads to spectral copies of only primary signals around modulation frequencies f_{mod} and higher harmonics.

1.2 Beam-hardening Correction for Semi-Transparent Squares

As described above, for spatial primary modulation (SPM) a primary modulator is inserted into the X-ray cone-beam in front of the sample. It imprints a regularly spaced intensity pattern onto primary radiation through the process of attenuation at the semi-transparent (dark) squares. For this reason, primary modulators are fabricated as etched printed circuit boards (PCB) with dark squares being made of copper and bright squares of epoxy resin prepreg, the first featuring high, the latter low attenuation. While the effect of beam hardening (BHD) is negligible for bright squares, it is not for the dark squares where the incident spectrum is hardened by e.g. 0.7mm of additional copper.
Let us consider how this affects the scatter calculation process by SPM. Since the spectrum behind dark squares has a greater mean energy as it would have if BHD was not occurring, X-rays passing through dark squares subsequently have greater penetration capabilities than without BHD. Consequentially, hardened primary X-rays irradiating the sample give rise to primary signals greater than they should be. During the demodulation process this leads to an estimate of the primary image which underestimates true primary signals. Thus, the scatter estimate will result in scatter signals which are too large. In the literature, this effect

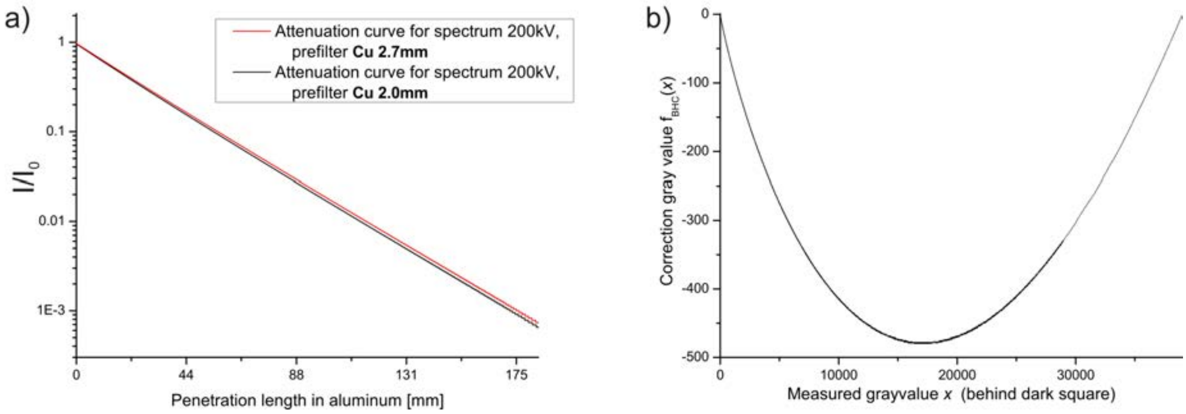

Figure 3. a) Attenuation curves simulated for two different spectra incident on aluminum wedge: For the primary modulators' bright squares we assume a spectrum pre-filtered by the tube prefilter of 2.0 mm (black), while for the dark squares the prefilter is effectively enlarged to 2.7 mm (red). b) From the difference between the two attenuation curves in a), we construct a lookup table which maps each originally measured gray value x to a correction value $f_{BHC}(x)$.

has been acknowledged but not been taken into account until very recently when Gao *et al* proposed to reduce BHD effects by selecting an optimal material for the primary modulator's dark squares [12]. This appears to be erbium for medical applications operating at 120kVp.

Alternatively and focused on industrial applications operating at greater voltages, we want to introduce a simple, simulation-based beam-hardening correction for dark squares which is applied –in a similar fashion– to entire CT projections in industrial CT. A limitation of the so-called linearization approach presented by Hammersberg *et al* [13] is that it is theoretically correct only for single-material samples. Therefore, here we consider single-material samples only, for demonstration purposes e.g. samples made of pure aluminum. For this situation, a given polychromatic X-ray spectrum of e.g. 200 kVp, and a tube prefilter of e.g. 2 mm of copper we can simulate two attenuation curves for X-rays irradiating an aluminum wedge sample: One for the group of bright squares where the spectrum incident on the sample is the input spectrum pre-filtered by 2 mm of copper and another one for the group of dark squares realized by e.g. 0.7 mm thick copper where the corresponding spectrum is effectively pre-filtered by 2.7 mm of copper. Figure 3a depicts the two attenuation curves on a logarithmic scale for I/I_0. As penetration lengths increase the difference in the two attenuation curves increases as well. From the simulated attenuation curves we construct a lookup table, shown in Fig. 3b, which maps each possibly measured, original gray value x from regions shadowed by dark squares to a correction value $f_{BHC}(x)$. Before projections are processed for spatial primary demodulation, we perform a BHD correction for all pixels (x,y) shadowed by dark squares. This involves the following steps:

- Given a total signal $T(x,y)$ at pixel (x,y), subtract a scatter estimate $S_{est}(x,y)$, e.g. by using the calculated scatter image from the CT projection before,
$$T'(x,y) = T(x,y) - S_{est}(x,y) \quad .$$
- Use $T'(x,y)$ as a lookup value in the lookup table f_{BHC}, this yields a (negative) correction value which is added to $T'(x,y)$ to yield $T'_{corr}(x,y)$,
$$T'_{corr}(x,y) = T'(x,y) + f_{BHC}[T'(x,y)] \quad .$$
- Undo subtracting the scatter estimate to yield the BHD corrected gray value for pixel (x,y), $$T_{corr}(x,y) = T'_{corr}(x,y) + S_{est}(x,y) \quad .$$

2. Experimental Setup

For preliminary demonstration of scatter correction by spatial primary modulation (SPM) combined with the beam-hardening (BHD) correction for dark squares we use an industrial CBCT scanner equipped with a 225 kV X-ray tube and a flat-panel detector. The sample is an aluminum test phantom of total dimensions 18 x 8 x 4 cm^3, including boreholes in one plane, which is tomographed with low magnification, i.e. the axis of rotation is located 15cm from the detector. CT scan parameters are: tube voltage 200 kVp, anode current 375 µA, prefilter of 2 mm of copper, 1080 CT projections.
In accordance to Section 1.2, we use a primary modulator fabricated as checkerboard pattern on a PCB with 99 x 99 squares, dark squares made of copper with thickness of 0.7 mm which results in approximately 20% attenuation. First, we perform a CT scan with the primary modulator in place and –for comparison– scatter correction is demonstrated for a single projection with and without BHD correction for darks squares, respectively. Second, a normal CT scan without the primary modulator is performed for comparison with the scatter-corrected CT scan in order to demonstrate the overall capability of scatter correction.

3. Experimental Results

3.1 Effect of Beam-hardening Correction for Semitransparent Squares in Scatter Images

Figure 4 shows calculated scatter images without BHD correction on the left-hand side and with BHD correction in the middle. Corresponding line profiles are given on the right-hand side for both cases and, as reference, also for a Monte-Carlo simulated scatter image where X-ray parameters are chosen accordingly. As we can see the BHD correction for dark squares results in smaller calculated scatter signals compared to the situation without BHD correction. This is in agreement to the expected behavior discussed in Section 1.2. Quantitatively, the line profiles indicate reduced scatter signals of 25% at the center and of about 40% in outer regions.

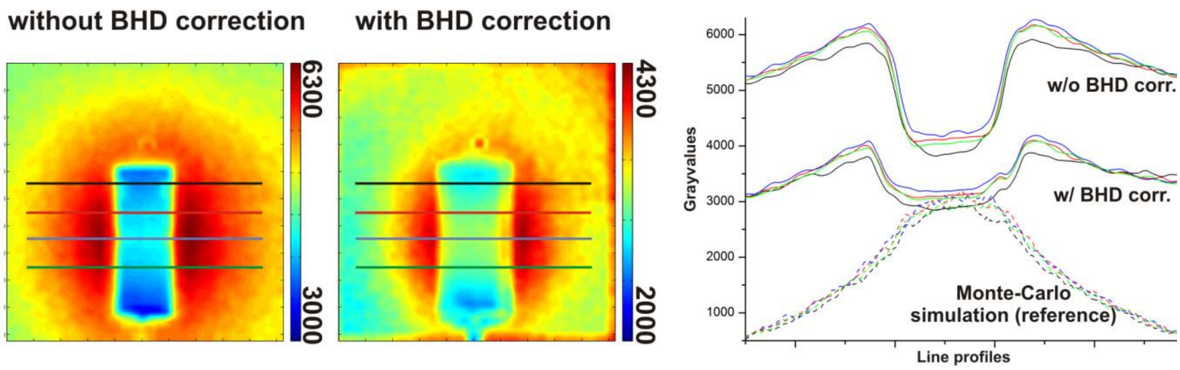

Figure 4. Calculated scatter images without beam-hardening (BHD) correction (left), with BHD correction (middle) and corresponding line profiles. For reference, corresponding line profiles from a Monte-Carlo simulated scatter image are also given. BHD correction for scatter calculation leads to smaller scatter gray values, in accordance to Monte-Carlo simulated scatter gray values (at the center, i.e. behind the object).

Furthermore, we notice good agreement of BHD-corrected scatter signals with corresponding Monte-Carlo simulated scatter signals in central regions which correspond to the sample's shadow. However, in outer regions these two differ strongly in magnitude. In fact, we see a steep increase in the measured line profiles in regions where a hard transition in the original CT projection is found also (mainly due to edges of the sample). Such a behavior of the scatter function has been identified to originate from strong contributions of detector internal scatter [1,9].

3.2 Experimental CT Results Demonstrating Scatter Correction using Spatial Primary Modulation

For comparison, Fig. 5 displays CT slices from the scatter corrected CT volume where spatial primary modulation is applied in combination with BHD correction as described in Section 1.2 (Fig. 5a) and from the uncorrected CT volume (Fig 5b). Significant improvements in image quality are observed for the scatter corrected CT compared to the uncorrected CT slice which shows typical scatter artifacts, e.g. streaks, cupping, and loss of contrast. The line profiles in Fig. 5c for the scatter corrected CT slice (black) and the uncorrected CT slice (red) also quantitatively indicate a strong correction of the scatter cupping artifact and recovery of optimized contrast at the center borehole.

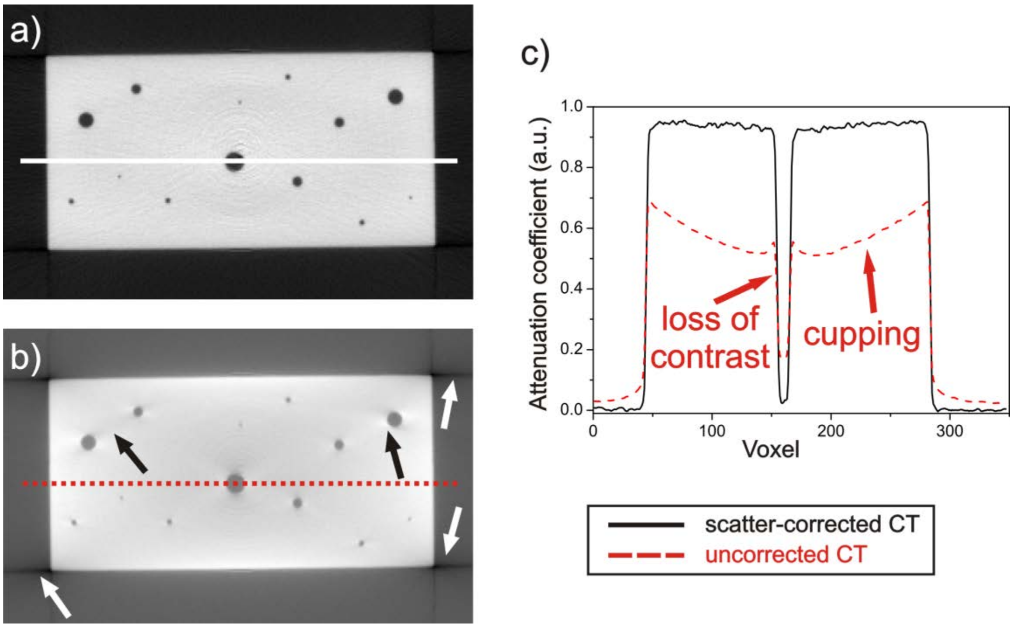

Figure 5. a) CT slice from scatter corrected CT volume showing nearly no scatter artifacts. b) Corresponding CT slice from normal CT scan without scatter correction. Typical scatter artifacts, e.g. streaks are indicated by arrows. c) Corresponding line profiles show a cupping artifact and loss of contrast for the uncorrected CT whereas the scatter corrected CT appears significantly improved at these points.

Conclusion

A new scatter correction method based on spatial primary modulation by insertion of a primary modulator into the beam path was proposed recently by the groups of Bani-Hashemi [10] and Zhu [11]. A great advantage of the method they propose lies in the fact that it can be included into a normal CT scan whereby additional scan time and effort are made obsolete. We implemented this form of scatter correction in our industrial CBCT scanner and examined the effects of beam hardening occurring at the dark squares. If left uncorrected, beam hardening will disturb the scatter estimation process rendering estimated

scatter signals too large. In order to correct for this effect we adopted a beam-hardening correction based on the linearization approach usually applied in the CT reconstruction process. For single-material samples this approach is theoretically correct and complete. We demonstrated a significant change in scatter signals when we apply our beam-hardening correction which leads to reduced scatter signals in the range of 25–40% in an exemplary projection.
Finally, we demonstrated significant improvement in CT image quality when scatter correction using spatial primary modulation combined with the proposed beam-hardening correction is performed. This includes strong reduction of the typical cupping artifact, enhanced contrast as well as elimination of streaks in CT slices.

Acknowledgements

We wish to thank Prof. Dr. Böni of Technische Universität München and Dr. Maltz of Siemens Medical Solutions (USA) for helpful discussions and support.

References

[1] Schörner K, Goldammer M, Stephan J: *Comparison between beam-stop and beam-hole array scatter correction techniques for industrial X-ray cone-beam CT*. Nucl. Instr. and Meth. B **269**, pp. 292–299 (2011).

[2] Bronnikov AV, Killian D: *Cone-beam tomography system used for non-destructive evaluation of critical components in power generation*. Nucl. Instr. and Meth. A **422**, pp. 909–913 (1999).

[3] Johns PC, Yaffe M: *Scattered radiation in fan beam imaging systems*. Med. Phys. **9**, pp. 231–239 (1982).

[4] Joseph PM, Spital RD: *The effects of scatter in x-ray computed tomography*. Med. Phys. **9,** pp. 464–472 (1982).

[5] Endo M, Tsunoo T, Nakamori N, Yoshida K: *Effect of scattered radiation on image noise in cone beam CT*. Med. Phys. **28**, pp. 469–474 (2001).

[6] Schörner K, Goldammer M, Stephan J: *Streustrahlenmessung und -korrektur durch Beamhole-Array und Beamstop-Array*. In Proceedings of Industrielle Computertomografie Tagung, 27-29 Sep 2010, Wels, Austria, pp. 235–242 (2010).

[7] Sorenson JA, Floch J: *Scatter rejection by air gaps. An empirical model*. Med. Phys. **12**, pp. 308–316 (1985).

[8] Ning R, Tang X, Conover D: *X-ray scatter correction algorithm for cone beam CT imaging*. Med. Phys. **31**, pp. 1195–1202 (2004).

[9] Peterzol A, Létang JM, Babot D: *A beam stop based correction procedure for high spatial frequency scatter in industrial cone-beam X-ray CT*. Nucl. Instr. and Meth. B **266**, pp. 4042–4054 (2008).

[10] Bani-Hashemi A, Blanz E, Maltz J, Hristov D, Svatos M: *Cone Beam X-Ray Scatter Removal Via Image Frequency Modulation and Filtering*. Med. Phys. **32**, p. 2093 (2005).

[11] Zhu L, Bennett NR, Fahrig R: *Scatter Correction Method for X-Ray CT Using Primary Modulation: Theory and Preliminary Results.* IEEE Trans. Med. Imaging **25**, pp. 1573–1587 (2006).

[12] Gao H, Zhu L, Fahrig R: *Modulator design for x-ray scatter correction using primary modulation: material selection*. Med. Phys. **37**, pp. 4029–4037 (2010).

[13] Hammersberg P, Mangard M: *Correction for beam hardening artifacts in computerised tomography*. J. X-Ray Sci. Technol. **8**, pp. 75–93 (1998).